Vertical Incidence Backscatter and Surface Forward Scattering From Near-Surface Bubbles

by S.O. McConnell and P.H. Dahl

Technical Report
APL-UW TR 9022
February 1991

Contract N00039-88-C-0054

Acknowledgments

This research was supported by the Office of Naval Technology with technical management by the Naval Oceanographic and Atmospheric Research Laboratory, Code 240 (R. Farwell). The authors especially thank Eric Thorsos and Kou-Ying Moravan of APL-UW for many helpful discussions.

TABLE OF CONTENTS

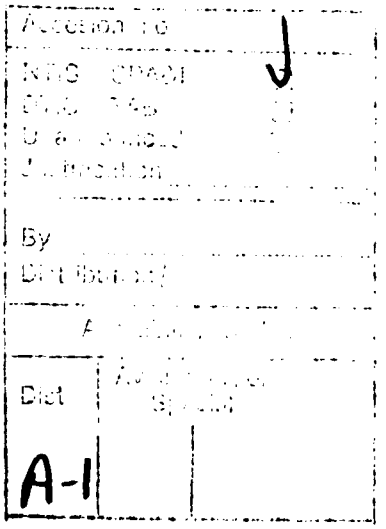

LIST OF FIGURES

I. EXECUTIVE SUMMARY

APL-UW made acoustic measurements of near-surface bubbles in fetch-limited shallow water in January and February 1986 as part of the High Frequency (10 to 500 kHz) Acoustics Project managed by NOARL. This work is applicable to torpedo guidance, control, and countermeasure technologies, and particularly to evaluating detection and signal-processing constraints imposed by a near-surface environment.

Bubbles near the surface were observed indirectly by measuring vertical incidence backscatter from the near-surface volume and producing vertical scattering strength profiles. Bubbles were observable from these measurements at wind speeds as low as 3 m/s. Surface forward scattering measurements at low grazing angles were also taken. The computed decibel loss from the forward scattering measurements, attributable to bubbles and referred to as surface bubble loss (SBL), was greater than 10 dB for wind speeds greater than about 5 m/s. Direct estimates of the integrated volume scattering strength σ_I were obtained from vertical incidence measurements (VI data), and inferred estimates of σ_I were obtained from the SBL estimates derived from the forward scattering loss measurements (FL data). The principal results are

(1) The depth dependence of the near-surface volume scattering strength followed the expected exponential behavior in the majority of cases, but significant departures occurred in some cases where a two-part exponential behavior is observed.

(2) The frequency dependence of σ_I derived from VI data was $\sigma_I \propto f^{2.4}$; the frequency dependence of σ_I inferred from FL data was $\sigma_I \propto f^{0.6}$.

(3) The wind speed dependence of σ_I derived from VI data was $\sigma_I \propto U^{6.1}$; the wind speed dependence of σ_I inferred from FL data was $\sigma_I \propto U^{2.2}$.

(4) The differences in the VI and FL data noted in (2) and (3) may in part be due to the VI data being less sensitive than the FL data to the near-surface bubble layer.

The data presented here represent a modest sampling of conditions in fetch-limited seas. These conditions differ from those in the open ocean, e.g., in the length scales of sea surface waves and characteristics of bubble plumes, so wind speed and frequency power laws reported here may also differ from those in the open ocean.

II. INTRODUCTION

This report presents results of acoustic measurements of vertical incidence backscattering and forward loss from near-surface bubbles. The measurements were made off Whidbey Island in Puget Sound in January and February 1986 using 1 ms pulsed cw signals with center frequencies ranging from 15–50 kHz. This work is part of the High-Frequency Acoustics Project (administered by the Naval Oceanographic and Atmospheric Research Laboratory), which primarily involves exploratory development within the frequency range of 10 to 500 kHz. Developments are applied to torpedo guidance and control and countermeasure technologies, such as detection and processing in a near-surface environment. A companion report (Dahl and McConnell, 1990) covers horizontal and vertical spatial coherence measurements made at the same experimental site. Here, we combine and extend earlier results from this experiment presented by McConnell (1988a,b).

III. EXPERIMENTAL ARRANGEMENT

Figure 1 shows the measurement location off Whidbey Island in Puget Sound. We chose this site for its fairly open exposure to passing storms at varying fetches up to 50 km (for winds from the west). Mile long cables connected the acoustic and environmental instrumentation to a shore site trailer containing electronic systems, computer, and recorders.

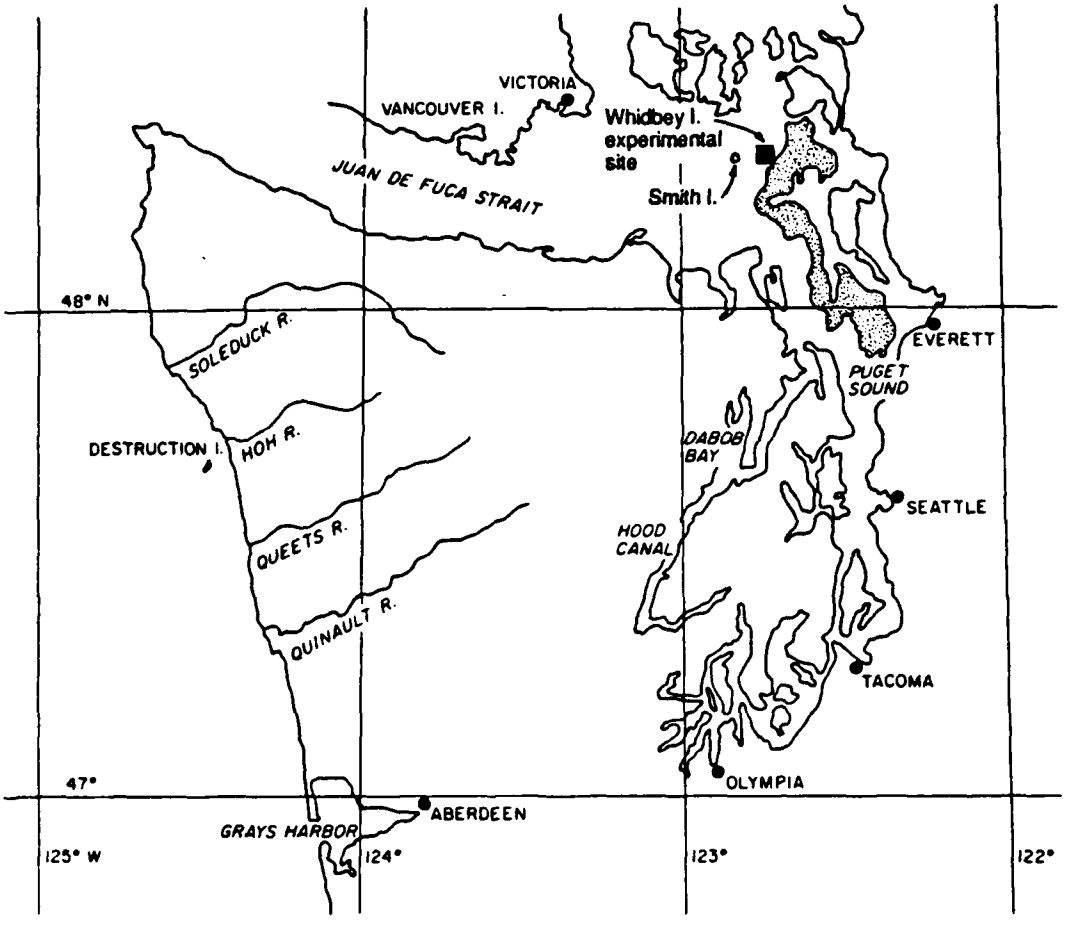

Figure 1. Experiment site off Whidbey Island in Puget Sound.

Data reported here were collected under winter environmental conditions characterized by mean wind speeds ranging from 0–15 m/s, with gusts recorded up to 23 m/s, and rms wave heights ranging from 2–50 cm. The wind speed data originate from the

National Ocean Survey's Smith Island recording station (about 4 miles from the experimental site) and from a cup anemometer located on shore. The Smith Island data are an average over 1 hour measured approximately 5 m from the sea surface, and the cup anemometer data are an average over approximately 10 minutes. All wind speeds reported here have been converted to the standard value of 10 m above the sea surface using the method of Smith (1988). We determined the rms surface wave height from the travel time fluctuations produced by the air–sea interface return from the vertical incidence backscatter signal. Typical air temperatures ranged from 4° to 9°C, with the sea temperature near the surface being a steady 4.35°C. The sound speed profile was measured during the course of the experiment using CTD casts. The winter conditions caused strong mixing within the water column, resulting in a nearly isovelocity profile of mean speed 1460 m/s.

The measurement geometry is shown in Figure 2. We made vertical incidence measurements using two 1.3 m long, linear arrays mounted perpendicular to each other atop a 5 m tripod tower on the seabed. Acoustic pulses were transmitted on one array and received on the other, producing a very narrow combined beam with a 3 dB beamwidth ranging from 1.2° at 50 kHz to 4.1° at 15 kHz. The frame on which the transducers were mounted could be varied in elevation (0° to 90°) and azimuth (300° total). The principal type of measurement was vertical incidence backscatter at 15–50 kHz using narrow beams and short pulse lengths. From these data we determined the near-surface volume scattering strength profile attributable to bubbles.

The volume scattering strength profile can be related to the scattering strength for an arbitrary bistatic geometry and therefore the surface forward loss. To test this relation, we interspersed surface forward scattering loss measurements at low grazing angle (plus one low angle backscatter measurement) with the vertical incidence measurements. For the surface forward scattering measurements we placed a nearly omnidirectional source 5 m above the bottom at a range of 500 m from the tower as depicted in Figure 2. Signals were received by a nearly omnidirectional hydrophone placed next to the line arrays on the tower. The alignment of the acoustic source and receiver was roughly parallel to the shoreline. Winds were primarily offshore or onshore, so the wave crests were approximately parallel to the direction of acoustic propagation. Because of the 35 m water depth, the receiver detected a number of multipath arrivals, including the single surface bounce path of primary interest. The dominant arrival involving the surface is this single bounce path since paths involving the bottom suffer a high loss owing to the porosity (0.7) of the soft mud at the measurement site.

Both the vertical incidence backscatter and surface forward scattering measurements used a sequence of 100 short pulses for each data set. For the first part of the experiment the data were recorded digitally at a single frequency. Pure tone pulses with lengths of 0.3 ms and 1 ms were interleaved and transmitted at a rate of one every 2 s,

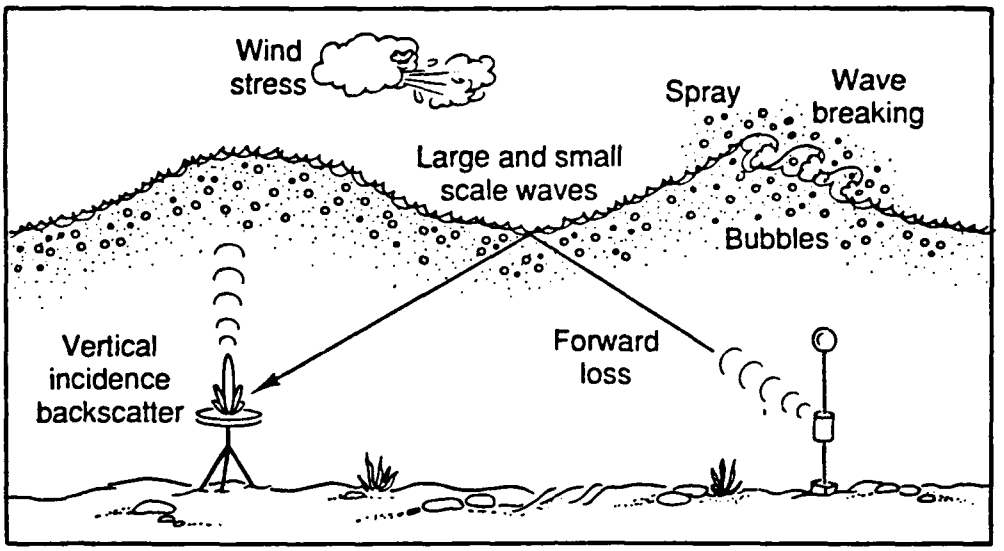

Figure 2. Sketch of the measurement geometry for vertical incidence backscattering measurements using two perpendicular line arrays, and forward loss measurements using a broadbeam transmitter and receiver. Also shown are the physical processes responsible for producing and influencing near-surface bubbles associated with wave breaking.

giving a total averaging time of 200 s for 50 pings of the same pulse length. The shorter pulse length data were used primarily to distinguish multipaths and are not discussed here. During the latter part of the experiment, the digital data acquisition system became inoperable owing to power failures, and data were recorded on analog tape using a sequence of seven different frequencies ranging from 15 to 45 kHz in 5 kHz steps. A 1 ms pulse length was used, and the time between pulses of different frequencies was 100 ms. Each sequence of pulses was transmitted once every 1.5 s, for a total averaging time of 150 s.

To obtain the average scattered intensity, a thresholding technique was devised to align the pings in time. Thresholding for the forward scattered signal was performed on the combined direct and single bottom bounce paths (time difference less than 0.1 ms between paths). This removed travel time variations due to motion of the transmitter in the tidal currents. The strong air–sea interface return was used for thresholding in the vertical incidence measurements. Thus the scattering strength profile could be determined as a function of depth below the instantaneous sea surface, rather than the mean sea surface. When the bubble density and receiver gain were high (thus saturating the

air–sea interface return), it was difficult to implement this thresholding technique on the vertical incidence signal. The difficulty arose when the bubble signal level became comparable to the interface signal level, and the bubble signal, rather than the interface signal, triggered the threshold. In such cases a large proportion of individual pings had to be carefully examined to determine the proper temporal shift.

IV. EXPERIMENTAL RESULTS

The vertical incidence backscatter results will be presented first, followed by the forward scattering loss measurements. Table 1 summarizes all the data and the corresponding environmental conditions in chronological order.

Table 1. Acoustic data parameters and environmental conditions.

Run No.	Frequency (kHz)	σ_f (dB)	σ_0, σ_1 (dB re m^{-1})	L_0, L_1 (m)	z_B (m)	*SBL* (dB)	Wind *Speed* ($m\ s^{-1}$)	*Wind* Direction	rms Wave *Height* (m)
43	30	-29.2	-27.0	0.61	---	---	13	W	0.34
44	30	-29.4	-34.4,-39.1	6.3,0.61	4.27	---	13	W	0.40
47	30	-23.6[a]	---	---	---	23.1	13	W	---
48	30	-24.6	-22.5,-38.0,-40.5	0.61,6.3,0.61	2.05,6.2	---	13	W	0.50
57	25	-21.0	-25.0,-34.6	2.49,1.26	5.1	---	13.5	W	0.66
60	25	-25.2[a]	---	---	---	15.0	13.5	W	---
62	25	-24.8	-23.9	0.82	---	---	13.5	W	0.51
67	20	-34.3	-30.1	0.45	---	---	10.8	W	0.44
68	20	-26.0[a]	---	---	---	11.5	10.8	W	---
72	20	-37.9	-38.1	1.05	---	---	10.8	SW	0.38
75	30	-37.5	-37.6,-40.5	2.67,0.39	1.32	---	13	SW	0.36
78	40	-32.4	-32.1,-44.8	1.00,0.38	2.67	---	13	SW	0.47
83	20	-52.9	-49.2	0.36	---	---	7.6	SE	0.10
84	30	-42.1	-40.3	0.66	---	---	7.6	SE	0.10
88	40	-40.1	-40.1,-44.7	1.79,0.42	1.48	---	7.6	SE	0.10
89	50	-36.5	-34.0	0.57	---	---	7.6	SE	0.10
91	50	---	---	---	---	0.5	4.5	SE	0.02
134	50	-25.3	-29.5,-41.4	3.10,0.57	5.82	---	*12.0*	*SE*	*0.17*
135	20	-30.1	-29.0	0.79	---	---	12.0	SE	0.17
136	40	-25.2	-26.5,-32.9	1.91,0.52	2.35	---	12.0	SE	0.17
137	30	-31.1	-29.4	0.67	---	---	12.0	SE	0.17
138	25	-23.5	-19.1	0.46	---	---	12.0	SE	0.17
139	50	-24.0	-24.5,-40.6	1.21,0.61	3.16	---	12.0	SE	0.17
32-1	20	-37.1	-33.6	0.44	---	---	12.4	SE	0.18
32-1	25	-26.5	-24.6,-44.0	0.69,0.33	2.19	---	12.4	SE	0.18
32-1	30	-36.1	-34.1	0.63	---	---	12.4	SE	0.18
32-1	35	-32.1	-26.3	0.26	---	---	12.4	SE	0.18
32-1	40	-31.0	-30.9	0.97	---	---	12.4	SE	0.18
32-8	20	-38.4	-35.2	0.51	---	---	12.4	SE	0.18
32-8	25	-27.7	-22.4	0.30	---	---	12.4	SE	0.18
32-8	30	-35.8	-31.4	0.37	---	---	12.4	SE	0.18
32-8	35	-31.2	-27.3	0.42	---	---	12.4	SE	0.18
32-8	40	-31.2	-27.9	0.47	---	---	12.4	SE	0.18
32-8	45	-27.0	-24.8	0.61	---	---	12.4	SE	0.18
32-3	15	-29.8[a]	---	---	---	5.5	12.4	SE	---
32-3	20	-29.0[a]	---	---	---	7.3	12.4	SE	--
32-3	25	-28.8[a]	---	---	---	8.2	12.4	SE	---
32-3	30	-28.0[a]	---	---	---	10.5	12.4	SE	---
32-3	35	-26.8[a]	---	---	---	14.4	12.4	SE	---
32-3	40	-26.7[a]	---	---	---	12.7	12.4	SE	---
32-10	20	-30.9[b]	---	---	---	---	12.4	SE	---
32-10	30	-30.2[b]	---	---	---	---	12.4	SE	---
32-10	40	-28.7[b]	---	---	---	---	12.4	SE	---
31-10	20	-44.7	-40.0	0.35	---	---	9.2	E	0.10
31-10	25	-43.9	-39.7	0.38	---	---	9.2	E	0.10
31-10	30	-41.4	-39.6,-47.0	0.81,0.26	1.42	---	9.2	E	0.10
31-10	35	-38.9	-35.7	0.48	---	---	9.2	E	0.10
31-10	40	-39.8	-38.4	0.74	---	---	9.2	E	0.10
31-10	45	-34.5	-35.6	1.31	---	---	9.2	E	0.10
31-12	20	-30.9[a]	---	---	---	4.7	9.2	E	---
31-12	30	-30.2[a]	---	---	---	6.3	9.2	E	---
31-12	40	-28.7[a]	---	---	---	9.9	9.2	E	---

[a] Inferred σ_f using surface bubble loss

[b] Inferred σ_f using low grazing angle backscatter

A. Vertical Incidence Backscatter

The average volume scattering strengths at 50 kHz and 20 kHz and two wind speed conditions (2 and 12 m/s) are shown in Figure 3 as a function of travel time. This travel time is equivalent to depth from the instantaneous sea surface when referenced to the air–sea interface return. Note that when the conditions are nearly calm no discernible bubble return is observed, and the leading edge of the air–sea interface return is sharp, rising 40 dB in about 1/3 ms. This clearly indicates that bubbles produced by mechanisms other than wave breaking (MacIntyre, 1986) are negligible. This simplifies the data analysis and allows us to focus solely on bubbles created by wave breaking and their acoustical effects. At a relatively high wind speed of 12 m/s the bubble returns are plainly visible above the background signal level at both 20 kHz and 50 kHz. The expected exponential rise in scattering level can be seen at 20 kHz from the straight line visual fit to the data. In the 50 kHz data there is a significant change in slope of this line; e.g., in the top line the fitted exponential depth constant decreases from 3.10 to 0.57 m. Thus at 50 kHz the behavior of the differential backscattering cross section per unit volume σ_s due to bubbles as a function of depth is described as follows:

$$\sigma_s = \begin{cases} \sigma_0 e^{-z/L_0} & , \ 0 < z < z_B \\ \sigma_1 e^{-z/L_1} & , \ z_B < z < \infty , \end{cases} \tag{1}$$

where z is positive downward from the sea surface, and z_B represents a break in the exponential decay profile. The other variables in Eq. (1) are discussed further in Appendix A. Most often the data evidenced an exponential profile (see Table 1; entries with a single depth constant, L_0), but two-segment profiles like those shown in Figure 3 were relatively common, and in one case a three-segment profile was observed. The deviation from an exponential profile tended to occur more often at higher wind speeds and frequencies. We note that the exponential profile is consistent with previously reported trends in bubble population data, e.g., Wu (1981) and Kerman (1986).

A convenient and informative method for condensing the data for each run to a single number is to compute the integrated volume scattering strength. This dimensionless quantity is found by integrating under the bubble return portion of the average profile shown in Figure 3. An example of this calculation is given in Appendix A. Figures 4 and 5 are examples of the integrated volume scattering strength covering the frequency range from 20–50 kHz and nominal wind speed range from 7.6–12.4 m/s (as measured from Smith Island). The expected increase in scattering level with wind speed is clearly evident. Data taken at wind speeds less than 3 m/s showed no measurable bubbles.

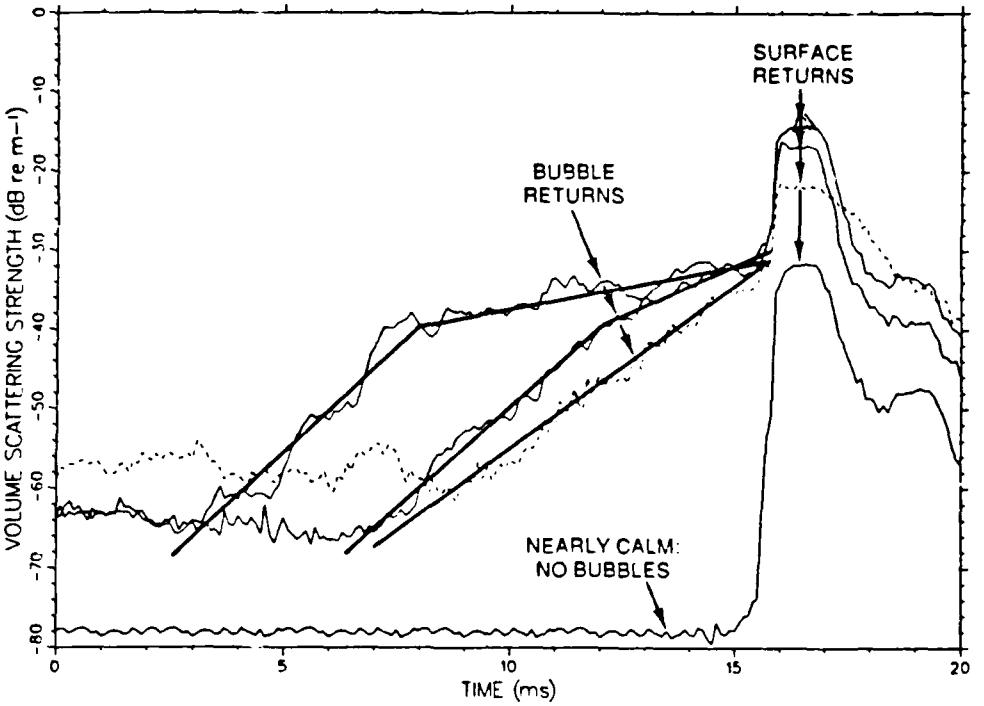

Figure 3. Volume scattering strength averaged over 50 pings (200 s) versus time into the ping cycle. The individual pings are aligned in time with respect to the instantaneous sea surface by thresholding on the surface returns. Three data runs at 50 kHz are shown as light solid lines, and one data run at 20 kHz is shown as a dashed line. The straight lines represent visual fits to the data. Bubbles are clearly visible for the two 50 kHz runs and one 20 kHz run taken at 12 m/s (labeled Bubble Returns); they are not visible on the 50 kHz run taken under nearly calm conditions (2 m/s). The nearly calm data have been adjusted down 15 dB.

The frequency dependence of the integrated volume scattering strength is also of interest. However, we expect σ_I to be a strong function of wind speed, and therefore small variations in U during the course of an experimental run can mask any trend with frequency. Obtaining the data in Figure 4 during the early part of the experiment took approximately an hour to cover the frequency range. Because those in Figure 5 were obtained during the latter part of the experiment (in the multifrequency mode), the same frequency range was covered in about 5 minutes. Thus we focus on Figure 5, which shows two runs taken at 12.4 m/s wind speed (separated in time by 50 minutes) and one run taken at 9.2 m/s. Although there is only one value available at 45 kHz, the two runs taken at 12.4 m/s are extremely consistent. The solid lines in the figure represent a power-law fit to the functional form

$$\sigma_I = \alpha f^m \qquad (2)$$

using the method of least squares. For the 9.2 m/s data the estimate for the parameter m is 2.60 (±1.5); for the 12.4 m/s data it is 2.8 (±1.9). We report the optimal values for the parameter estimates, with the bounds in parentheses representing the 95% confidence interval based on assumptions regarding the underlying distribution of the data (Bendat and Piersol, 1986). The 25 kHz data (Table 1, runs 32-8 and 32-1) were not included in the least squares analysis. We are not convinced that the unusually high values for σ_I at 25 kHz, measured during these runs as well as some earlier runs, are accurate; experimental records show an intermittent interference (of unknown source) centered near the 25 kHz band.

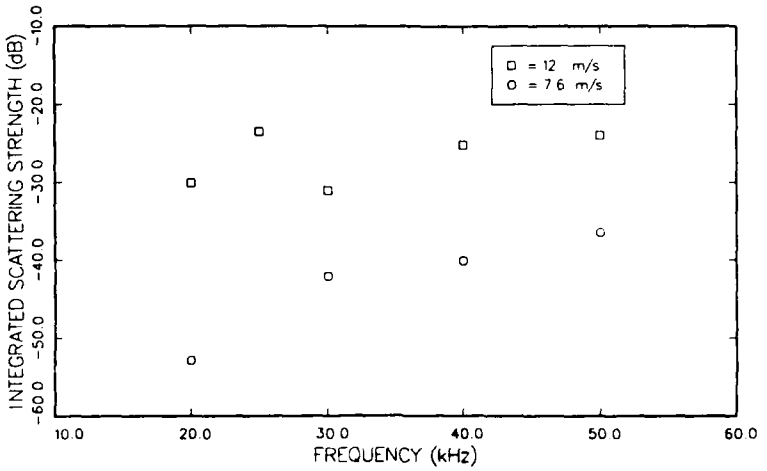

Figure 4. The integrated volume scattering strength attributable to bubbles versus transmit frequency, at two wind speeds.

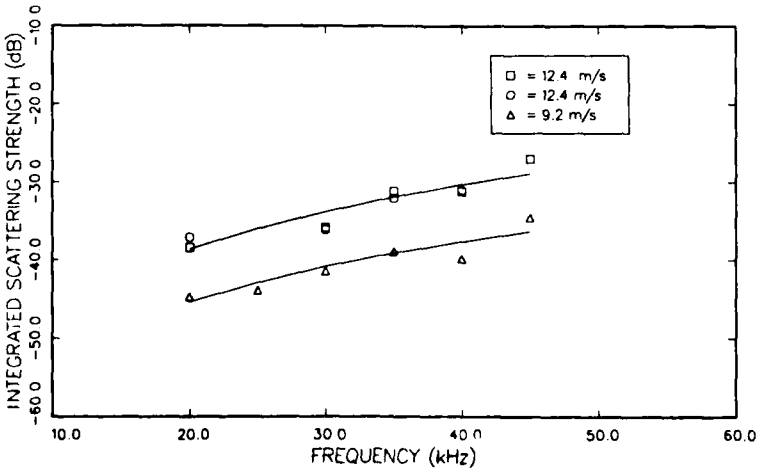

Figure 5. The integrated volume scattering strength attributable to bubbles versus transmit frequency. The upper set of data was taken at a wind speed of 12.4 m/s, and the lower set was taken at 9.2 m/s. The solid lines represent a least squares fit of Eq. (2) to the data.

Limited averaging time for the 50-ping runs can also lead to variations in the average σ_I values, particularly since the spatial sampling size was relatively small (surface patch size of about 1 m diameter). Figure 6 is an example of the variation in the integrated scattering strength as a function of time, taken during the early, single frequency part of the experiment. The interesting characteristic of the time variation of σ_I is that at the higher wind speeds there appear to be longer time scales of variation. Thus a longer time averaging period is necessary if the variance associated with the final mean value is to be reduced. The time for each run made at a single frequency cannot be extended, however, without risking significant changes in the environmental conditions.

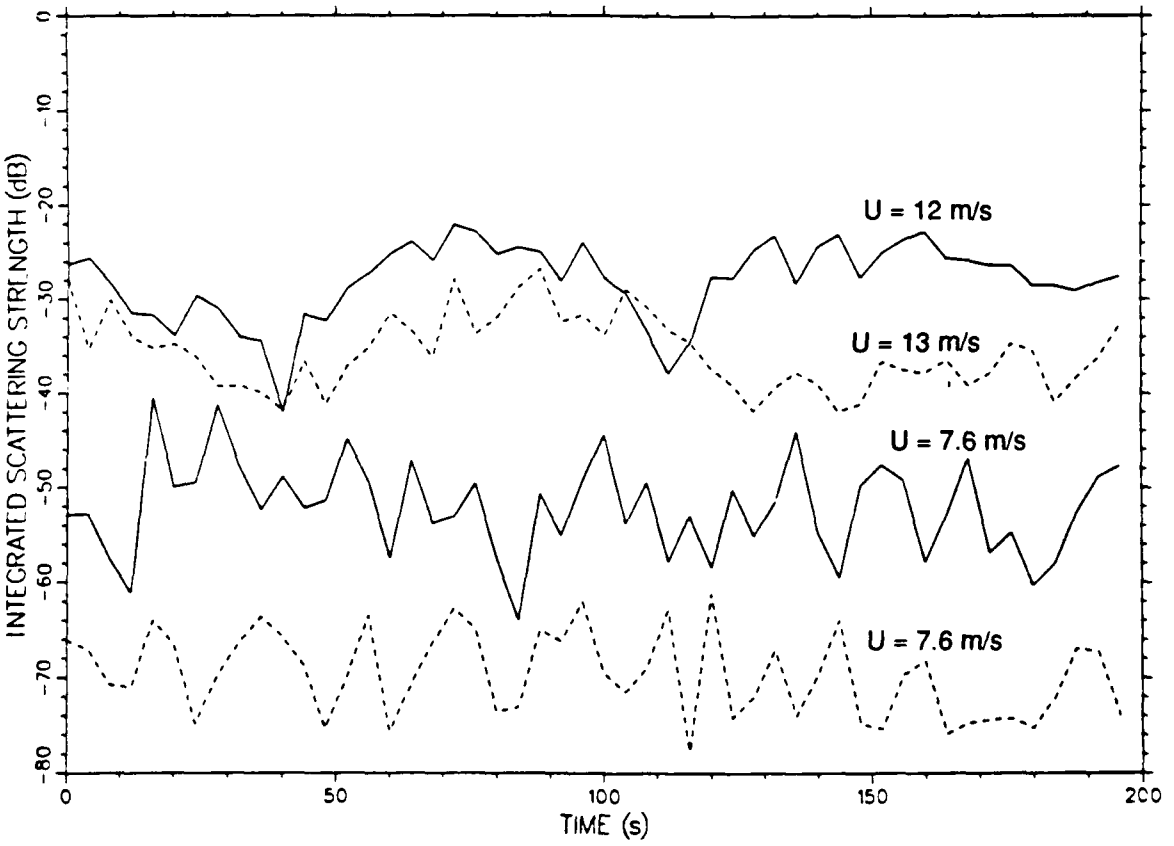

Figure 6. Time dependence of the individual (single ping) integrated volume scattering strengths as a function of wind speed. The 50 kHz data are shown as solid lines (lower curve is adjusted down 10 dB), and the 30 kHz data as dashed lines (lower curve is adjusted down 25 dB).

B. Surface Forward Scattering

Surface forward scattering measurements at low angles were interleaved between the vertical incidence measurements. Figure 7 shows two examples of the forward scattered signal, one for low wind speed and one for a relatively high wind speed. The combined direct and bottom bounce path signals are evident as the early, near-replica arrival, which is followed by the surface bounce and other multipath arrivals. The first surface bounce arrivals rapidly increase to a peak over a one-pulse-length period and then gradually decay beyond. With the low wind speed, another peak occurs at 12 ms following the direct path arrival, which is due to the multipaths involving two surface bounces. Note that the curve for the higher wind speed is about 10 dB lower in level and displays a much slower decay in level beyond the first peak; also, no second peak is visible.

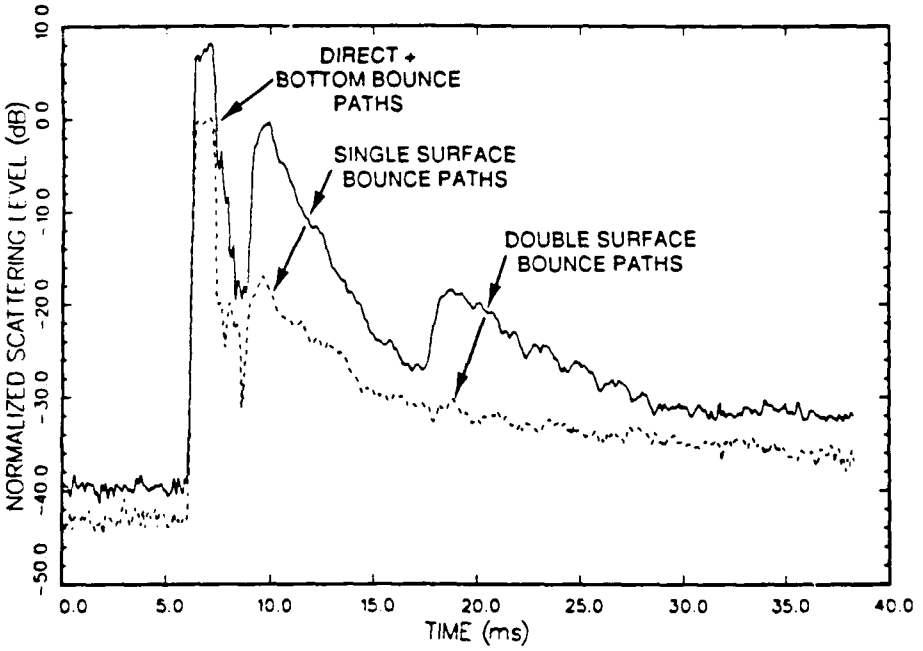

Figure 7. Normalized forward scattering level averaged over 50 pings (200 s) versus time into the ping cycle. The normalization is such that a single direct path should appear as a transmit pulse replica with a level of 0 dB if spherical spreading plus chemical absorption describes the path loss. The upper set of data was taken at 50 kHz with a wind speed of 4.5 m/s, and the lower set at 20 kHz and wind speed of 10.8 m/s.

The forward scattering loss due to a single surface bounce was computed by integrating the scattered intensity from the leading edge of the single-surface bounce arrivals to the leading edge of the double-surface bounce arrivals. From the decibel

equivalent of this integral, 1.5 dB is subtracted to account for the inclusion of arrivals involving bottom bounces. The 1.5 dB value is determined from the integrated intensity measured during calm conditions. In the absence of bubble attenuation the theoretical value for this loss is 0 dB; i.e., no loss is associated with scattering from the air–sea interface, and scattering is treated as a 0 dB reflection loss (Thorsos, 1984a). Any measured loss is then attributed to bubble attenuation effects and is referred to as surface bubble loss (SBL). For low wind speed the SBL was 0.5 dB (Table 1, run 91). For high wind speed the SBL was 11.5 dB (Table 1, run 68).

The integrated volume scattering strength computed from the vertical incidence backscatter measurements can be compared with this same quantity inferred from the surface forward scattering measurements. The inferred σ_I is calculated from the SBL estimates via the transfer function

$$\sigma_I \text{ [dimensionless]} = \frac{\sin\theta}{109.2} \frac{\delta_R}{\delta} SBL \text{ [dB]} , \tag{3}$$

where

$\delta = 2.55 \times 10^{-3} f^{1/3}$ (fit to data in Devin, 1959)
(total damping coefficient) ,

$\delta_R = 0.0136$
(radiation damping coefficient),

and

$\theta = 6.9°$
(grazing angle for single surface bounce).

This calculation is reviewed in Appendix B.

Figures 8 and 9 compare σ_I derived from direct vertical incidence measurements (VI) with that inferred from surface forward scattering loss measurements (FL) taken a few minutes apart. In Figure 9 we have also plotted estimates of σ_I derived from low-angle backscatter measurements for $\theta \approx 30°$ grazing angle, where backscattering strength is converted to σ_I following the method described by McDaniel (1988). The VI measurements in Figure 9 are an average of those shown in Figure 5, which were taken before and after the FL measurements. The solid lines represent a least squares fit of the data to Eq. (2). In this case $m = 0.7$* for the FL measurements taken at $U = 9.2$ m/s (Figure 8), and $m = 0.9$ (± 0.5) for the FL measurements taken at $U = 12.4$ m/s (Figure 9).

*The three FL data points in Figure 8 are not enough to compute a meaningful confidence interval about the optimum estimate.

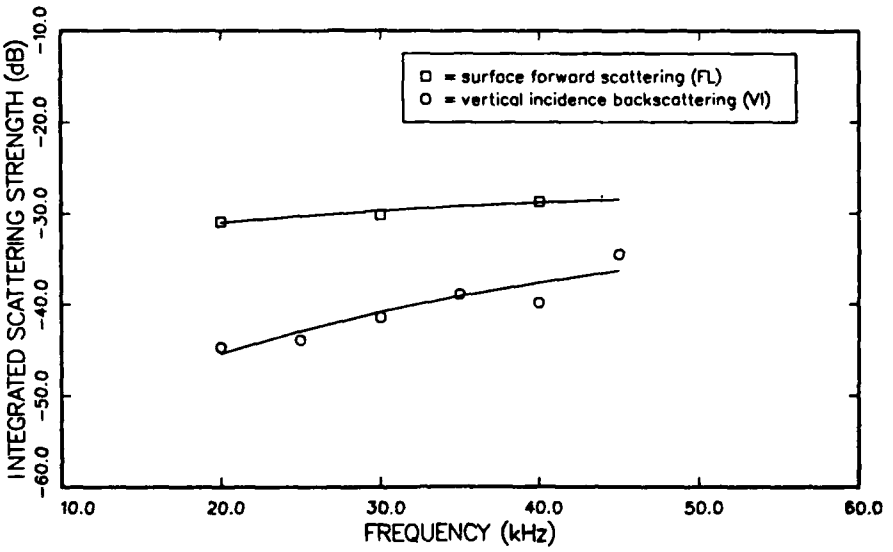

Figure 8. A comparison of the integrated volume scattering strength obtained directly from vertical incidence backscattering measurements (VI) with those inferred from surface forward scattering loss measurements (FL). The data were taken at a wind speed of 9.2 m/s. The solid lines represent a least squares fit of Eq. (2) to the data.

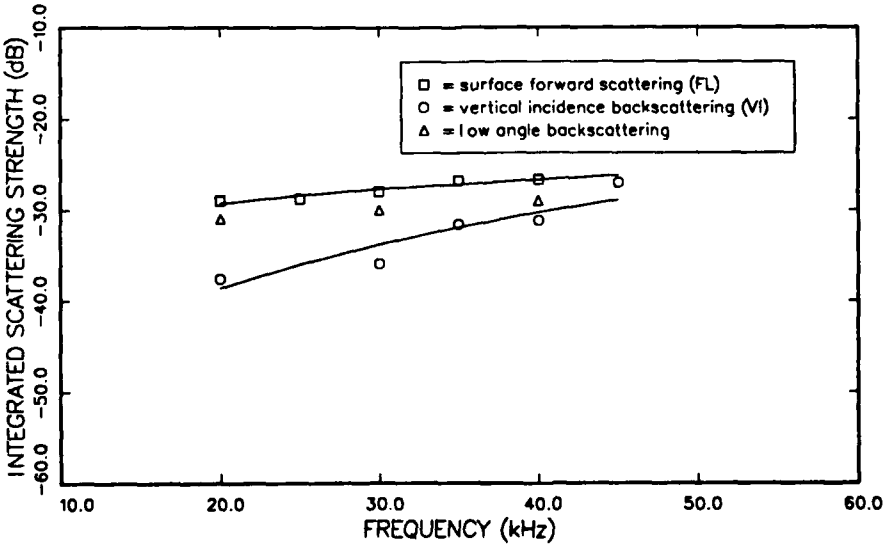

Figure 9. A comparison of the integrated volume scattering strength obtained directly from vertical incidence backscattering measurements (VI) with those inferred from surface forward scattering loss measurements (FL), and low-angle backscattering measurements. The data were taken at a wind speed of 12.4 m/s. The solid lines represent a least squares fit of Eq. (2) to the VI and FL data.

V. DISCUSSION AND SUMMARY

There is a significant offset between the VI and FL estimates of σ_I, but the FL and low angle backscatter-derived estimates are within experimental error of each other. The reason for this difference may lie in the existence of a thin (~ 10 cm) layer of high bubble concentration next to the air–sea interface. Such a near-surface layer has been observed and is termed the "bubble generation layer" (Baldy, 1988). The finite pulse lengths used in the VI measurements could not detect bubbles within such a thin layer and resolve them from the air–sea interface return—despite our attempts to correct for this, as discussed in Appendix A. On the other hand, both the FL and low-angle backscatter measurement techniques inherently sample this layer. An additional observation lending further support to the existence of such a layer is that the VI data slowly converge toward the FL data at the higher frequencies corresponding to smaller resonant bubble radii. These smaller bubbles have lower buoyancy rise rates, and thus have longer residence times below the sea surface and within a zone that can be resolved by the VI measurements. We also note that the smaller difference between the VI data and the FL data at the higher of the two wind speeds is suggestive of the downward displacement of a greater proportion of the bubbles as turbulent mixing increases with wind speed.

Returning to Figures 8 and 9, we note the difference in the frequency power laws for σ_I derived from VI and FL data; this difference is approximately 1.9 in the exponent m in Eq. (2) for both figures. An equivalent frequency power-law relation for N_R, the depth integrated bubble density at resonance, can be derived from Appendix B. The VI data show a frequency dependence for N_R of approximately f^6; for the FL data this dependence is approximately f^4. The frequency power law derived from FL data is consistent with the data of Farmer and Lemon (1984) taken at 14.5 kHz and 25 kHz. Furthermore, the frequency power law derived from VI data suggests that N_R falls off more rapidly with size than would be indicated by the FL data. This is also consistent with the VI approach not being sufficiently sensitive to the bubble population in the near-surface layer.

Finally, there is a significant difference in the wind speed dependence for the fitted curves shown in Figures 8 and 9. For example, for the wind speed change from 9.2 to 12.4 m/s, both the VI and FL fitted curves show a nearly constant displacement across the frequency range 20–40 kHz: about 6 dB for the VI data and about 2 dB for the FL data. In order to infer a wind speed power-law dependence while accounting for the frequency dependence, and thereby utilize all the data in Table 1, we proceed with a multivariable power-law fit to the functional form

$$\sigma_I = \beta f^m U^n \tag{4}$$

using the method of least squares. A new arbitrary constant β is used here to distinguish

it from the α in Eq. (2). The optimal estimate for the parameter m is 2.4 (±0.6) for the VI data and 0.6 (±0.4) for the FL data. In both cases the estimates lie within the confidence intervals computed using only the multifrequency data of Table 1 (from run 32-1 down), showing the consistency in the entire data set. The optimal estimate for the parameter n is 6.1 (±1.6) for the VI data, which indicates $\sigma_I \propto U^{6.1}$, or equivalently, $N_R \propto U^{6.1}$, and is consistent with data from Farmer and Lemon. On the other hand, for the FL data the optimal estimate for n is 2.2 (±1.6), indicating $\sigma_I \propto U^{2.2}$, or equivalently, $N_R \propto U^{2.2}$. However, other reports (e.g., Thorsos, 1984b) have shown surface forward scattering data similar to ours that are not uniquely determined by wind speed. Furthermore, comparisons and interpretations of the wind speed and frequency power laws reported here are tenuous because the fetch-limited conditions off Whidbey Island differ from those in the open ocean, e.g., in the length scales of sea surface waves and characteristics of bubble plumes.

In summary, it is clear from the vertical incidence measurements that bubbles are acoustically observable at wind speeds as low as 3 m/s and that for wind speeds greater than about 5–6 m/s the surface bubble loss (SBL) can become quite large (>10 dB). Direct estimates of the depth integrated volume scattering strength σ_I were obtained from vertical incidence measurements (VI data), and inferred estimates of σ_I were obtained from the SBL estimates associated with the low angle surface forward scattering loss measurements (FL data). In most cases the VI and FL measurements were separated in time by no more than a few minutes. The principal results are

(1) The depth dependence of the near-surface volume scattering strength followed the expected exponential behavior for the majority of cases, but significant departures occurred in some cases where a two-part exponential behavior is observed.

(2) The frequency dependence of σ_I derived from VI data was $\sigma_I \propto f^{2.4}$; the frequency dependence of σ_I inferred from FL data was $\sigma_I \propto f^{0.6}$.

(3) The wind speed dependence of σ_I derived from VI data was $\sigma_I \propto U^{6.1}$; the wind speed dependence of σ_I inferred from FL data was $\sigma_I \propto U^{2.2}$.

(4) The differences in the VI and FL data noted in (2) and (3) may in part be due to the VI data being less sensitive than the FL data to the near-surface bubble layer.

REFERENCES

Baldy, S., 1988: "Bubbles in the Close Vicinity of Breaking Waves: Statistical Characteristics of the Generation and Dispersion Mechanism," *J. Geophys. Res.*, **93**, 8239–8248.

Bendat, J. S., and A. G. Piersol, 1986: *Random Data: Analysis and Measurement Procedures*, 2nd ed., 105–107, Wiley, New York.

Dahl, P. H., and S.O. McConnell, 1990: "Measurements of Acoustic Spatial Coherence in a Near-Shore Environment," APL-UW TR 9016, Applied Physics Laboratory, University of Washington, Seattle.

Devin, C., Jr., 1959: "Survey of Thermal, Radiation, and Viscous Damping of Pulsating Air Bubbles in Water," *J. Acoust. Soc. Am.*, **31**, 1654–1667.

Farmer, D. M., and D. D. Lemon, 1984: "The Influence of Bubbles on Ambient Noise in the Ocean at High Wind Speeds," *J. Phys. Oceanogr.*, **14**, 1762–1778.

Hildebrand, F., 1976: *Advanced Calculus for Applications*, 367–368, Prentice-Hall, Englewood Cliffs, New Jersey.

Kerman, B. R., 1986: "Distribution of Bubbles Near the Ocean Surface," *Atmos.-Ocean*, **24**, 169–188.

MacIntyre, F., 1986: "On Reconciling Optical and Acoustical Bubble Spectra in the Mixed Layer," 75–94, in *Oceanic Whitecaps and Their Role in Air–Sea Exchange Processes*, E. C. Monahan and G. Mac Niocaill (eds), D. Reidel, Boston.

McConnell, S. O., 1988a: "Acoustic Measurements of Bubble Densities at 15–50 kHz," 237–252, in *Sea Surface Sound: Natural Mechanisms of Surface Generated Noise in the Ocean*, B. R. Kerman (ed.), Kluwer Academic, Boston.

McConnell, S. O., 1988b: "Backscattering and Forward Loss from Near-Surface Bubbles," *J. Acoust. Soc. Am., Suppl. 1*, **84**, S121.

McDaniel, S. T., 1988: "Acoustical Estimates of Subsurface Bubble Densities in the Open Ocean and Coastal Waters," 225–236, in *Sea Surface Sound: Natural Mechanisms of Surface Generated Noise in the Ocean*, B. R. Kerman (ed.), Kluwer Academic, Boston.

Medwin, H., 1977: "In Situ Acoustic Measurements of Microbubbles at Sea," *J. Geophys. Res.*, **82**, 971–976.

Smith, S.D., 1988: "Coefficients for Sea Surface Wind Stress, Heat Flux, and Wind Profiles as a Function of Wind Speed and Temperature," *J. Geophys. Res.*, **93**, 15,467–15,472.

Thorsos, E.I., 1984a: "Surface Forward Scattering and Reflection," APL-UW 7-83, Applied Physics Laboratory, University of Washington, Seattle.

Thorsos, E.I., 1984b: "High-Frequency Surface Forward-Scattering Measurements," *J. Acoust. Soc. Am.*, Suppl. 1, **76**, S55.

Urick, R.J., 1983: *Principles of Underwater Sound,* 3rd ed., 240–244, McGraw-Hill, New York.

Wu, J., 1981: "Bubble Populations and Spectra in Near-Surface Ocean: Summary and Review of Field Measurements," *J. Geophys. Res.*, **86**, 457–463.

APPENDIX A

This appendix discusses the variables in Eq. (1) and reviews the calculations involved in obtaining an estimate of σ_l. Figure A1 shows a profile of the reverberation level (in arbitrary decibel units) as a function of time. The profile rises exponentially above the noise level between the points marked by 2 and 1, owing to scattering from bubbles. We first determine an exponential depth constant L_o that governs the profile between points 1 and 2, such that

$$I_2 = I_1 e^{-z/L_o} . \tag{A1}$$

For example, for the levels shown in Figure A1 we find L_o= 0.303 m.

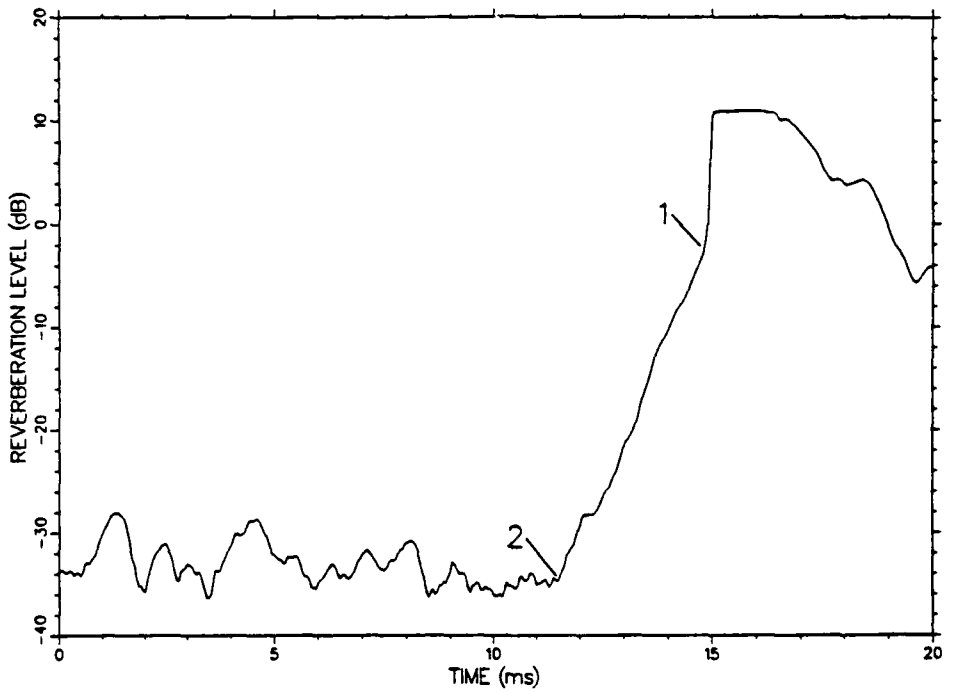

Figure A1. Profile of the reverberation level (in arbitrary decibel units) averaged over 50 pings versus time into the ping cycle. The behavior between points 1 and 2 is modeled as an exponential decay.

Next I_o, the maximum intensity in the reverberation profile, is determined. By hypothesis, I_o is due to backscattering from bubbles located immediately below the surface but not from the air–sea interface itself. That is, we remove the effects of sea surface backscatter in the midst of a reverberation producing volume. However, since the reverberation profile is dominated by the air–sea interface beyond point 1, we infer a

level for I_o by extending the exponential profile a distance $c\tau/4 = 0.364$ m beyond point 1. The distance $c\tau/4$ is used because it centers the equivalent scattering volume (producing I_o) at the air–sea interface. For this case we find $I_o = 3.6$ dB. By including system gains and receiving sensitivity, this is equivalent to a reverberation level RL_o = 120 dB re μPa.

The reverberation profile, which has now been extended to the air–sea interface, is converted to volume scattering strength S_{Vo} in a straightforward manner following Urick (1983). For example,

$$S_{Vo} = RL_o - SL + 40 \log R - 10 \log V \, . \tag{A2}$$

The relevant parameters for this example are SL = 204.8 dB re μPa and R = 29.8 m, with the scattering volume $V = (c\tau/2) R^2 \psi$, where ψ is the equivalent solid angle corresponding to the combined transmitting and receiving line arrays. We account for sound absorption in seawater and arrive at an initial estimate of the volume scattering strength for the near-surface layer due to bubbles. We refer to this as S'_{Vo}, which is equal to −23.4 dB re 1 m^{-1}, or equivalently $\sigma'_o = 0.00457$.

A final estimate of σ_o and σ_I must also include the effect of absorption due to bubbles. The two-way transmission loss due to bubbles is expressed as (Medwin, 1977)

$$TL_b = 8.686 \int_o^\infty \sigma_e (z) \, dz \, , \tag{A3}$$

where σ_e is the total extinction cross section per unit volume. The extinction and differential backscattering cross sections per unit volume due to bubbles are related by

$$\sigma_e = \sigma_s \, 4\pi \, \frac{\delta}{\delta_R} \, , \tag{A4}$$

where δ and δ_R are defined below Eq. (3). The depth dependence of σ_s usually assumes a single profile equal to $\sigma_o \, (e^{-z/L_o})$. In some cases the profile may consist of two parts involving σ_1 and L_1 as shown in Eq. (1). We use the single profile case in the integral in Eq. (A3) because σ_o is always much greater than σ_1, giving

$$TL_b = 8026 \, \delta \, \sigma_o \, L_o \, . \tag{A5}$$

Finally, an equation for a revised estimate of σ_o that includes the effect of bubble absorption is

$$10 \log \sigma_o = S'_{Vo} + 8026 \, \delta \, \sigma_o \, L_o \, . \tag{A6}$$

Equation (A6) has only one unknown, σ_o, which we readily solve numerically using the Newton-Raphson method (Hildebrand, 1976). The result for this example is S_{Vo} = −22.4 dB re 1 m^{-1}. Finally, σ_I is computed by depth integrating σ_s; e.g., in the single profile case we have

$$\sigma_I = \sigma_o L_o \, . \tag{A7}$$

APPENDIX B

This appendix reviews the means of conversion between SBL and σ_I. The backscattering cross section per unit volume due to entrained bubbles is (Medwin, 1977)

$$\sigma_s = \frac{3.4\pi}{4} A_R^3(z)\, N(A_R)/\delta\,, \tag{B1}$$

where A_R is the radius of resonant bubbles, $N(A_R)$ is the number of resonant bubbles per unit volume per unit bubble radius in microns, and δ is defined below Eq. (3). Medwin also shows that A_R (in microns) at depth z (in meters) is related to frequency (in kilohertz) by

$$A_R \approx \frac{3.25\,10^3}{f}\ \sqrt{1 + 0.1\,z}\ . \tag{B2}$$

By definition,

$$\sigma_I = \frac{3.4\pi}{4}\ \frac{1}{\delta}\ \int_o^\infty A_R^3(z)\, N(A_R)\, dz\ . \tag{B3}$$

Because A_R is slowly varying over the range of significant bubble concentration, we have

$$\sigma_I \approx \frac{3.4\pi}{4}\ \frac{1}{\delta}\ A_R^3\ \int_o^\infty N(A_R)\, dz\ . \tag{B4}$$

The integral in Eq. (B4) is defined as N_R, the depth-integrated bubble density at resonance. *SBL* is defined by Thorsos (1984a) as

$$SBL\ (\mathrm{dB}) = \frac{8.686}{\sin\theta} \int_d^\infty \sigma_e(z)\, dz\ . \tag{B5}$$

In our case we integrate from $d=0$. We note that SBL is just the two-way transmission loss due to bubbles, (Eq. A3), modified for arbitrary angle of incidence. From Eqs. (A4) and (B1), and carrying out the integration as in (B3), we find

$$SBL\ (\mathrm{dB}) = \frac{8.686}{\sin\theta}\ \frac{3.4\pi^2}{A_R^3(z)\,\delta_R}\, N_R\,, \tag{B6}$$

which leads to the transfer function, Eq. (3) in Section IV of the text.

UNCLASSIFIED

SECURITY CLASSIFICATION OF THIS PAGE

REPORT DOCUMENTATION PAGE

Form Approved OMB No. 0704-0188

1a REPORT SECURITY CLASSIFICATION: Unclassified

1b RESTRICTIVE MARKINGS:

2a SECURITY CLASSIFICATION AUTHORITY: NAVINST 5513.5A

2b DECLASSIFICATION / DOWNGRADING SCHEDULE:

3 DISTRIBUTION / AVAILABILITY OF REPORT: Approved for public release; distribution is unlimited.

4 PERFORMING ORGANIZATION REPORT NUMBER(S): APL-UW TR9022

5 MONITORING ORGANIZATION REPORT NUMBER(S):

6a NAME OF PERFORMING ORGANIZATION: Applied Physics Laboratory, University of Washington

6b OFFICE SYMBOL (If applicable):

7a NAME OF MONITORING ORGANIZATION:

6c ADDRESS (City, State, and ZIP Code): 1013 NE 40th Street, Seattle, WA 98105-6698

7b ADDRESS (City, State, and ZIP Code):

8a NAME OF FUNDING / SPONSORING ORGANIZATION: NOARL

8b OFFICE SYMBOL (If applicable): 240

9 PROCUREMENT INSTRUMENT IDENTIFICATION NUMBER: SPAWAR Contract N00039-88-C-0054

8c ADDRESS (City, State, and ZIP Code): Stennis Space Center, MS 39529-5004

10 SOURCE OF FUNDING NUMBERS

PROGRAM ELEMENT NO	PROJECT NO	TASK NO	WORK UNIT ACCESSION NO
602435N	RJ35V11		

11 TITLE (Include Security Classification): Vertical Incidence Backscatter and Surface Forward Scattering from Near-Surface Bubbles

12 PERSONAL AUTHOR(S): S.O. McConnell and P.H. Dahl

13a TYPE OF REPORT	13b TIME COVERED	14 DATE OF REPORT (Year, Month, Day)	15 PAGE COUNT
technical	FROM _____ TO _____	February 1991	26

16 SUPPLEMENTARY NOTATION:

17 COSATI CODES		
FIELD	GROUP	SUB-GROUP

18 SUBJECT TERMS (Continue on reverse if necessary and identify by block number): spatial coherence, vertical incidence backscattering, environmental acoustics, high frequency, near-surface bubbles, surface forward scattering

19 ABSTRACT (Continue on reverse if necessary and identify by block number)

This report presents results of acoustic measurements of vertical incidence backscattering and surface forward scattering from near-surface bubbles. The measurements were made off Whidbey Island in Puget Sound in January and February 1986. Applications of this work are directed toward torpedo guidance, control, and countermeasure technologies, such as detection and signal-processing constraints imposed by the near-surface environment. Acoustic measurements of the concentration and vertical extent of near-surface bubbles generated by breaking waves were made in the frequency range 15-50 kHz. The vertical incidence measurements, which were interspersed with the surface forward scattering measurements, produced a vertical profile of volume scattering cross section due to bubbles that decreased exponentially with depth. By integrating this profile in depth, a direct estimate of integrated

20 DISTRIBUTION / AVAILABILITY OF ABSTRACT: ☒ UNCLASSIFIED/UNLIMITED ☐ SAME AS RPT ☐ DTIC USERS

21 ABSTRACT SECURITY CLASSIFICATION: Unclassified

22a NAME OF RESPONSIBLE INDIVIDUAL: Robert W. Farwell

22b TELEPHONE (Include Area Code): (601) 688-4875

22c OFFICE SYMBOL: 240

DD Form 1473, JUN 86 — Previous editions are obsolete — S/N 0102-LF-014-6603

SECURITY CLASSIFICATION OF THIS PAGE

UNCLASSIFIED

19. Abstract (cont'd)

volume scattering strength σ_I was made, which is a measure of total bubble concentration. The surface forward scattering measurements show a loss for a single surface interaction. This loss, attributable to bubbles, is referred to as the surface bubble loss (SBL), and an inferred estimate of σ_I was obtained from the SBL through a transfer function that incorporates the total extinction cross section from bubbles.

The vertical incidence backscattering data and the forward scattering data, interpreted in terms of scattering and absorption by resonant bubbles, did not produce comparable trends in frequency and wind speed functional dependence, and differed significantly in overall level. For example, the forward scattering data indicate bubble concentrations that are as much as an order of magnitude greater than those indicated by the vertical incidence measurements. A likely explanation for the observed differences between the two data sets is discussed.